Support information

Peptide Dendritic Polymerization-Enabled Stable and Tailorable Nanoparticles as Crosslinkers for Fabricating Multifunctional Hydrogels with Enhanced Wound Healing Efficacy

Haonan Ye,[a] Zhanshan Gao ,[a] Yin Liu,[a] Jiahao Liu ,[a] Tianzi Chen,[a] Yueting Wei,[a] Han Zhao[a] and Dongdong Wu*[a]

[a] National Engineering Research Center for Biomaterials, College of Biomedical Engineering, Sichuan University, Chengdu 610064, China

E-mail: wudd@scu.edu.cn.

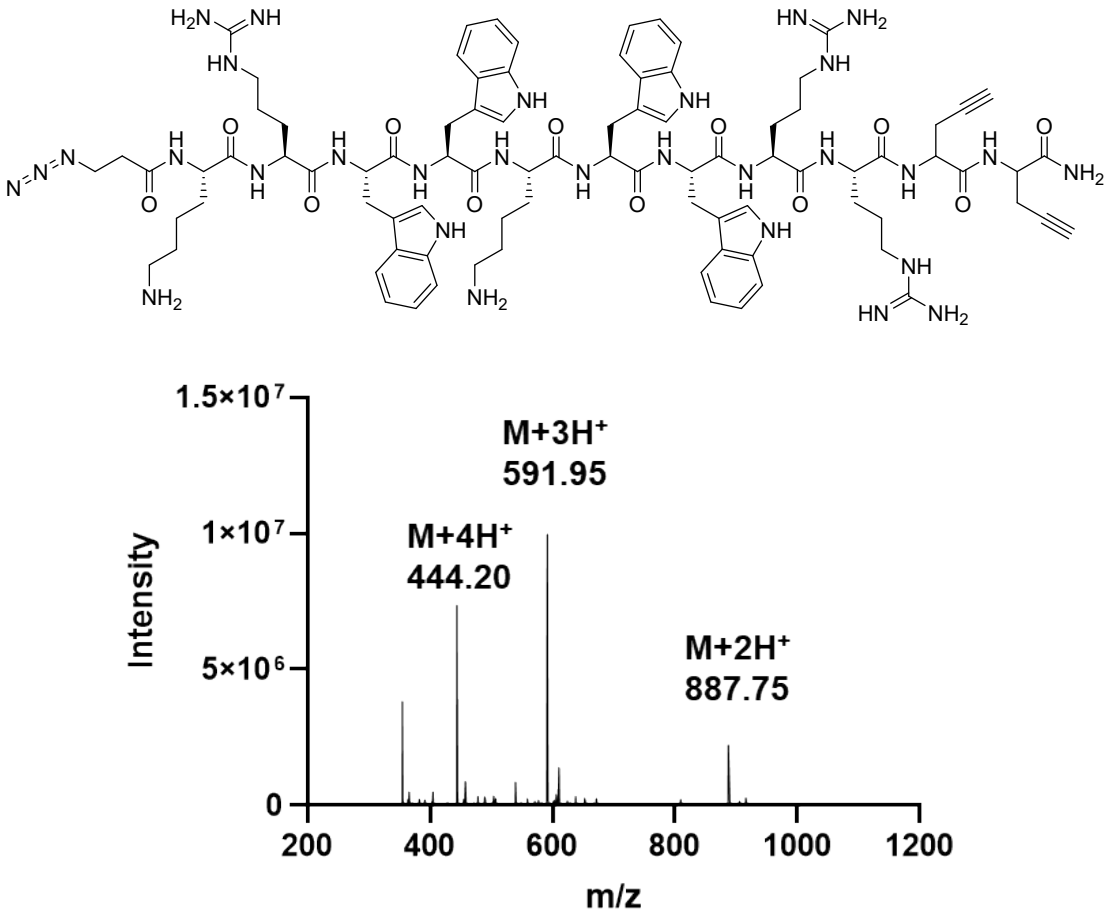

Figure S1. Mass spectrometric analysis of AB_2-type cationic peptide (**CP**) bearing an azide group at N-termini and two alkyne moieties at C-termini.

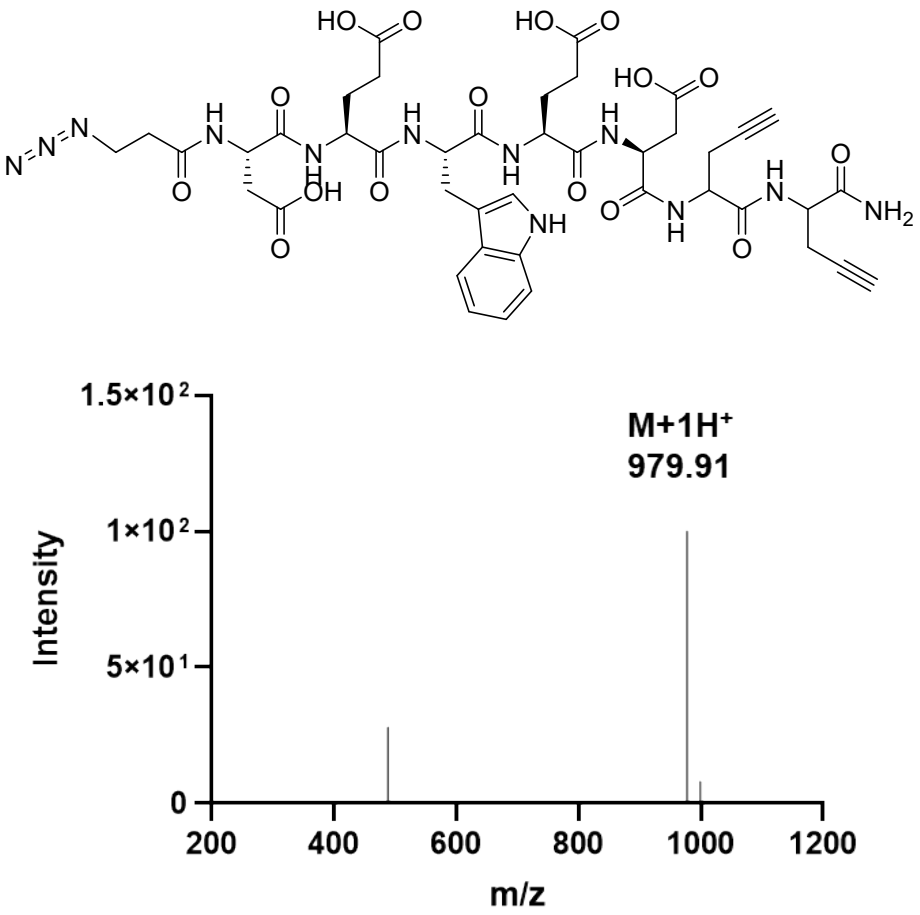

Figure S2. Mass spectrometric analysis of AB_2-type anionic peptide (**AP**) bearing an azide group at N-termini and two alkyne moieties at C-termini.

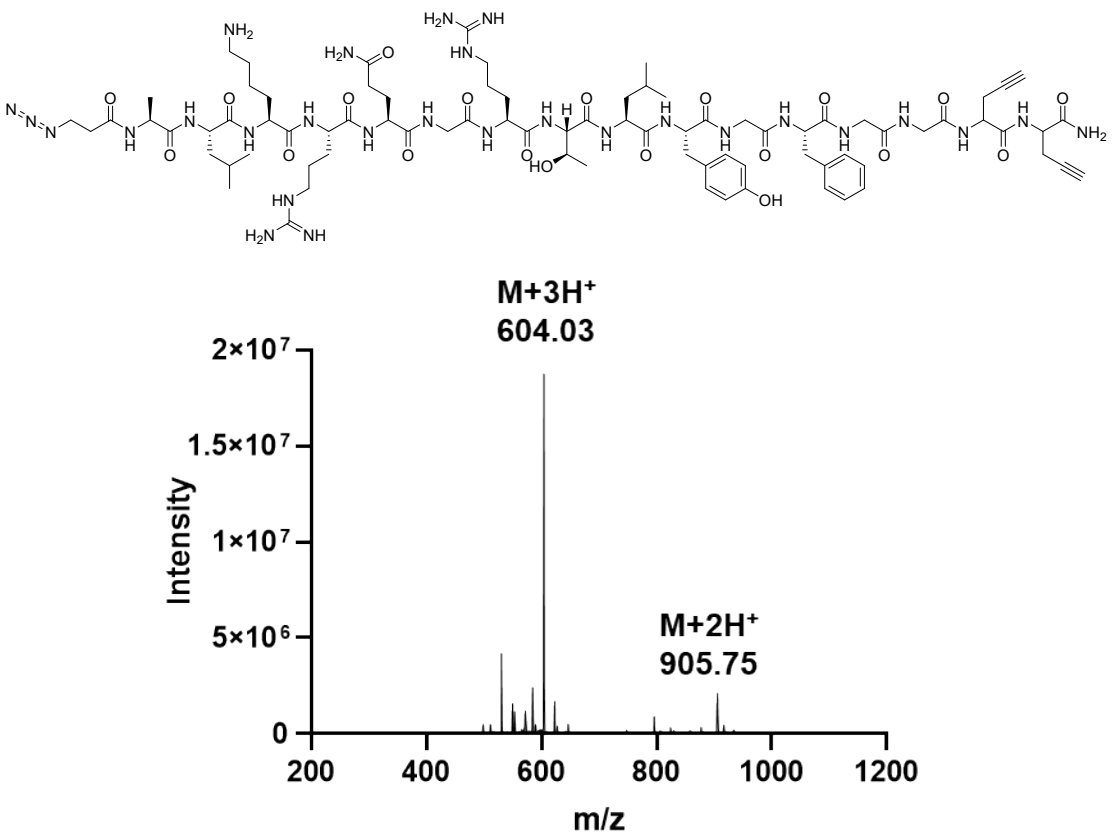

Figure S3. Mass spectrometric analysis of AB_2-type osteogenic growth peptide (**OGP**) bearing an azide group at N-termini and two alkyne moieties at C-termini.

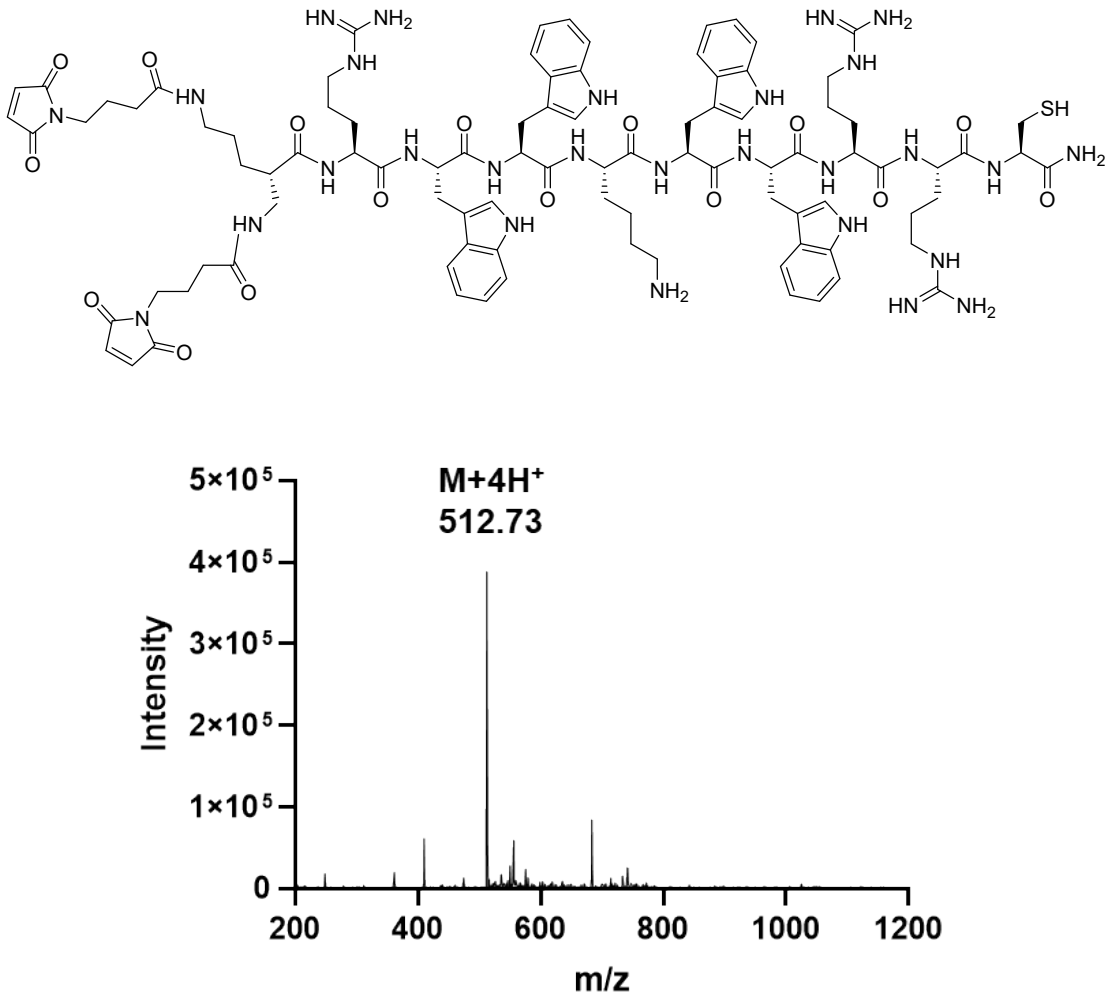

Figure S4. Mass spectrometric analysis of AB_2-type cationic peptide (**CP-1**) bearing two maleimide groups at N-termini and a thiol group at C-termini..

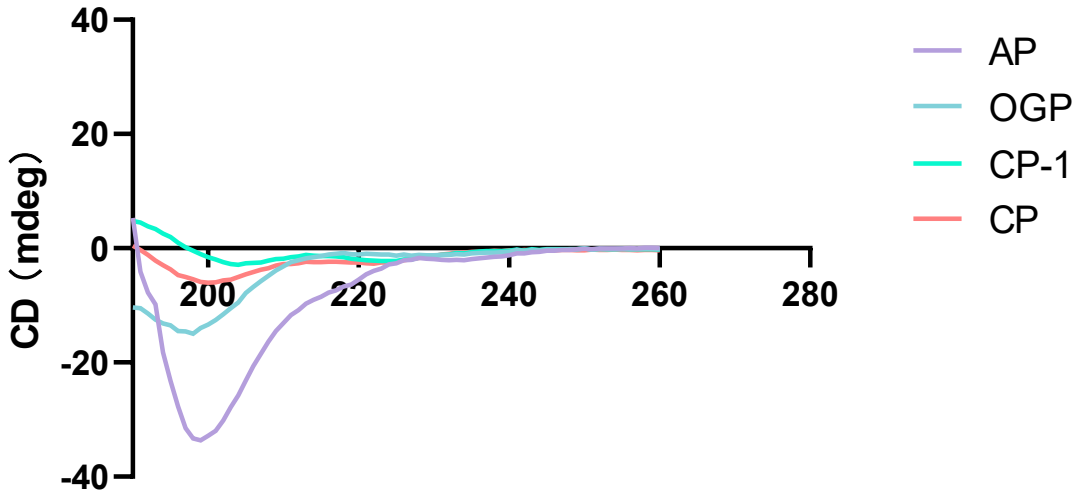

Figure S5. CD spectra of different peptides.

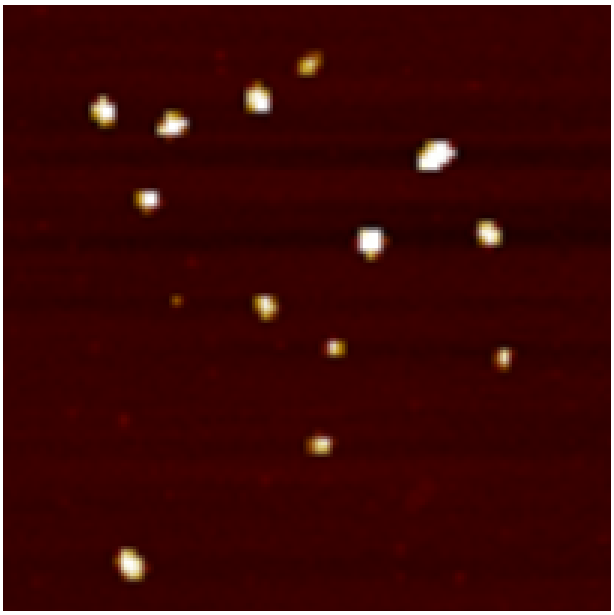

Figure S6. AFM image of cationic peptide nanoparticles (CPN)**.**

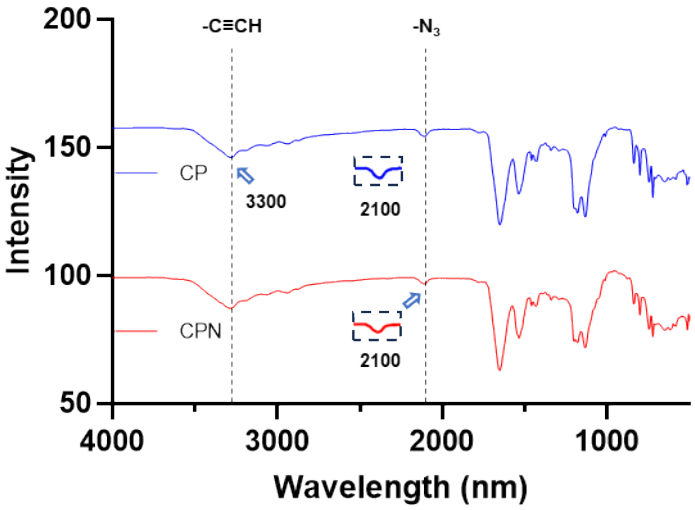

Figure S7. FT-IR spectra of CP and CPN.

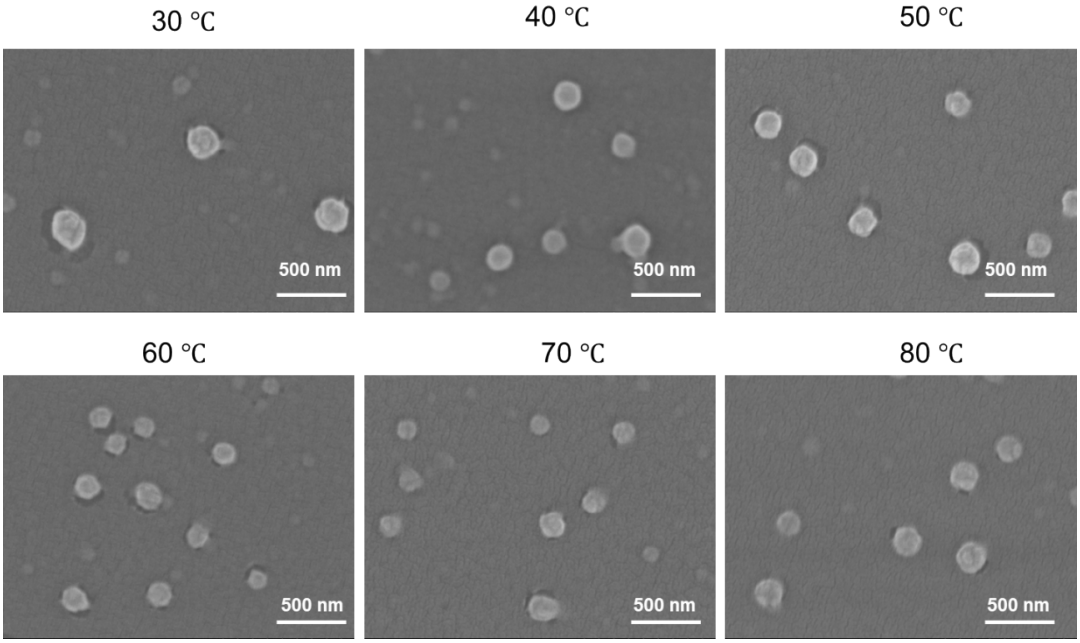

Figure S8. SEM images of CPN at different temperatures.

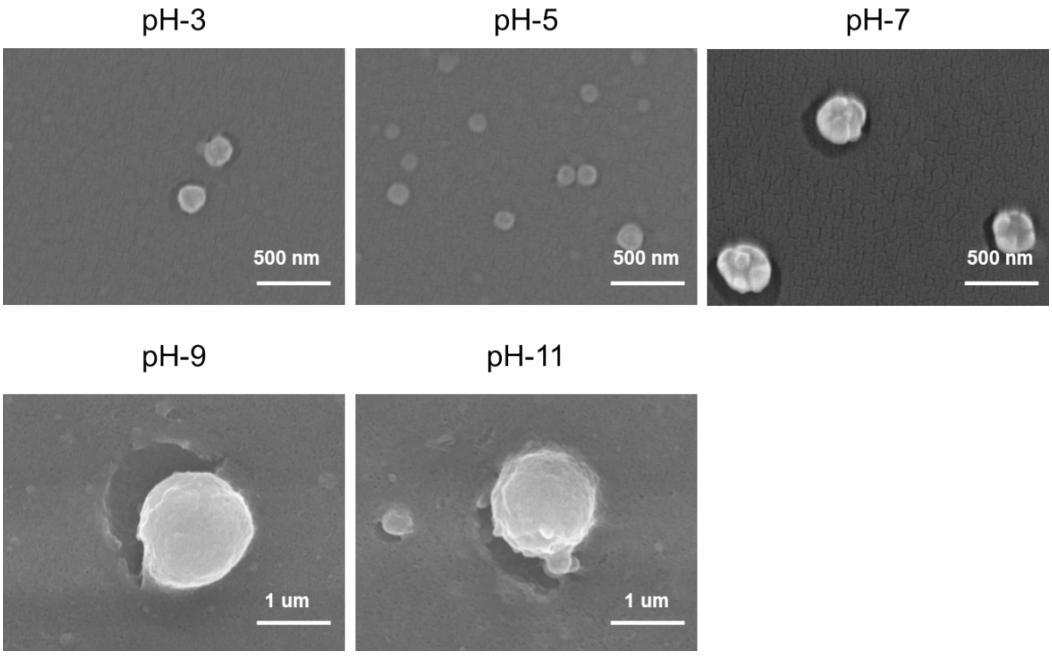

Figure S9. SEM images of CPN at different pH values.

Peptide type	Peptide sequence	A group	B group
Cationic (CP)	KRWWKWWRR	Azide	Alkyne
Anionic (AP)	DEWED	Azide	Alkyne
Osteogenic (OGP)	ALKRQGRTLYGFGG	Azide	Alkyne
Cationic (CP-1)	KRWWKWWRR	Thio	Maleimide

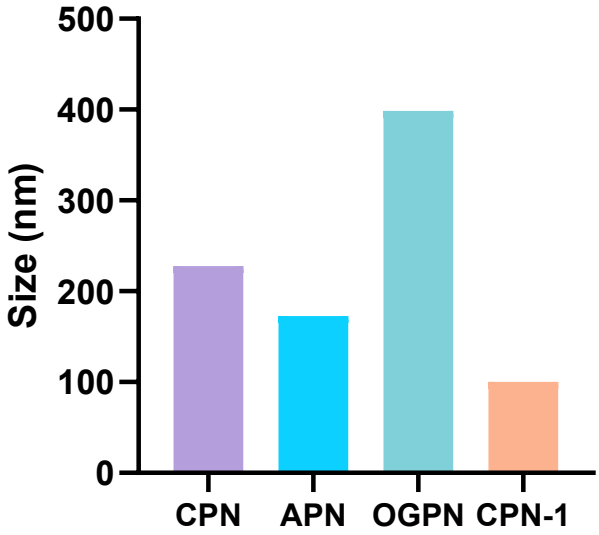

Figure S10. The average diameters of different peptide nanoparticles. Error bars represent standard deviation. For CPN, APN, and OGPN, data were obtained from DLS measurements (n = 3). For CPN-1, the diameter was determined by statistical analysis of TEM images (n ⩾ 50 particles).

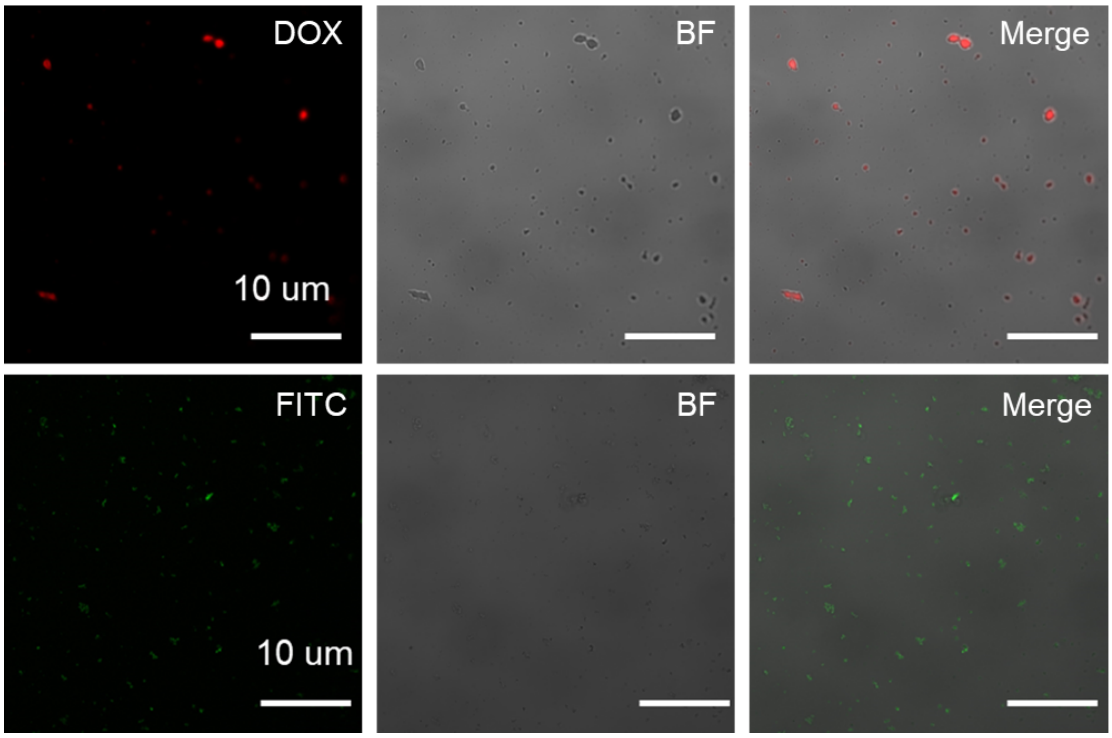

Figure S11. Confocal assessment of the post-functionalized nanomaterials.

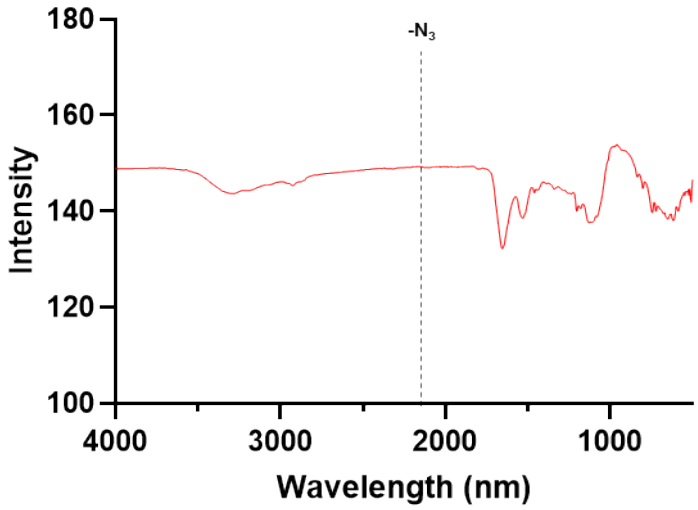

Figure S12. FT-IR spectrum of the CPN-PEG-FITC.

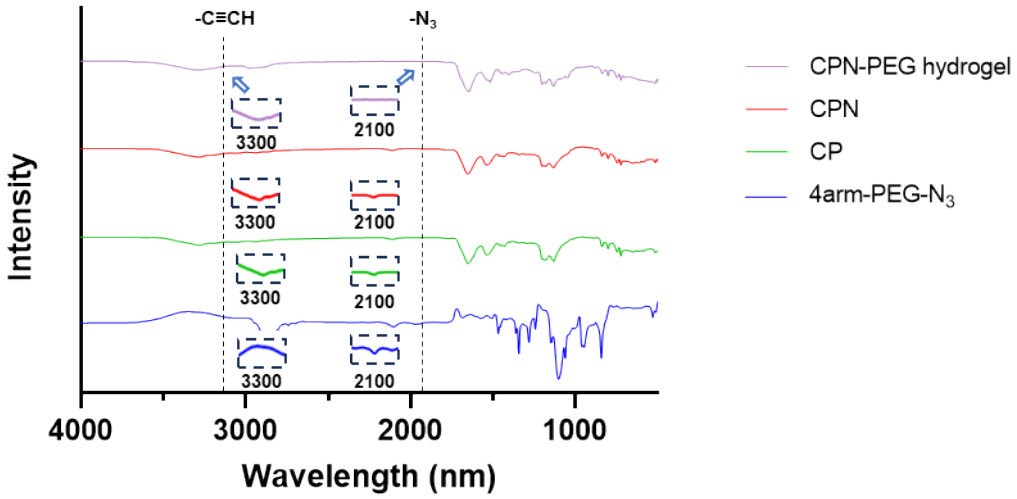

Figure S13. FT-IR analysis of CP, CPN, CPN-PEG hydrogel, and 4-arm-PEG-N_3.

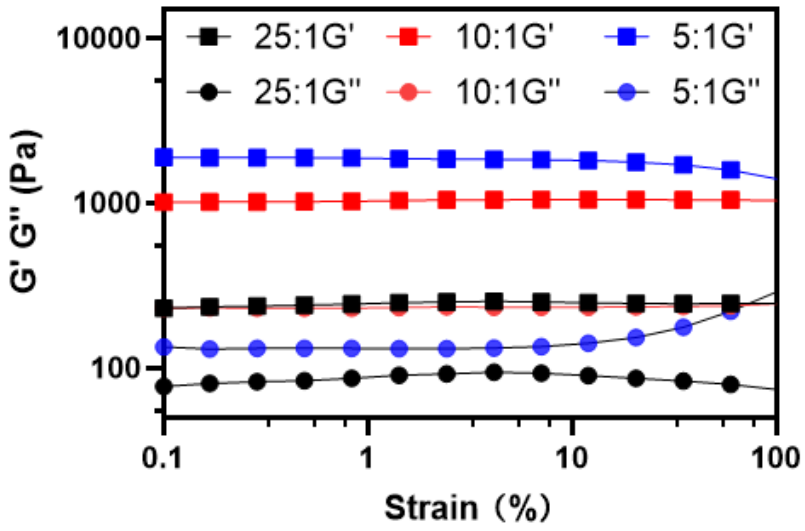

Figure S14. Strain sweep rheology of hydrogels with different cross-linking ratios.

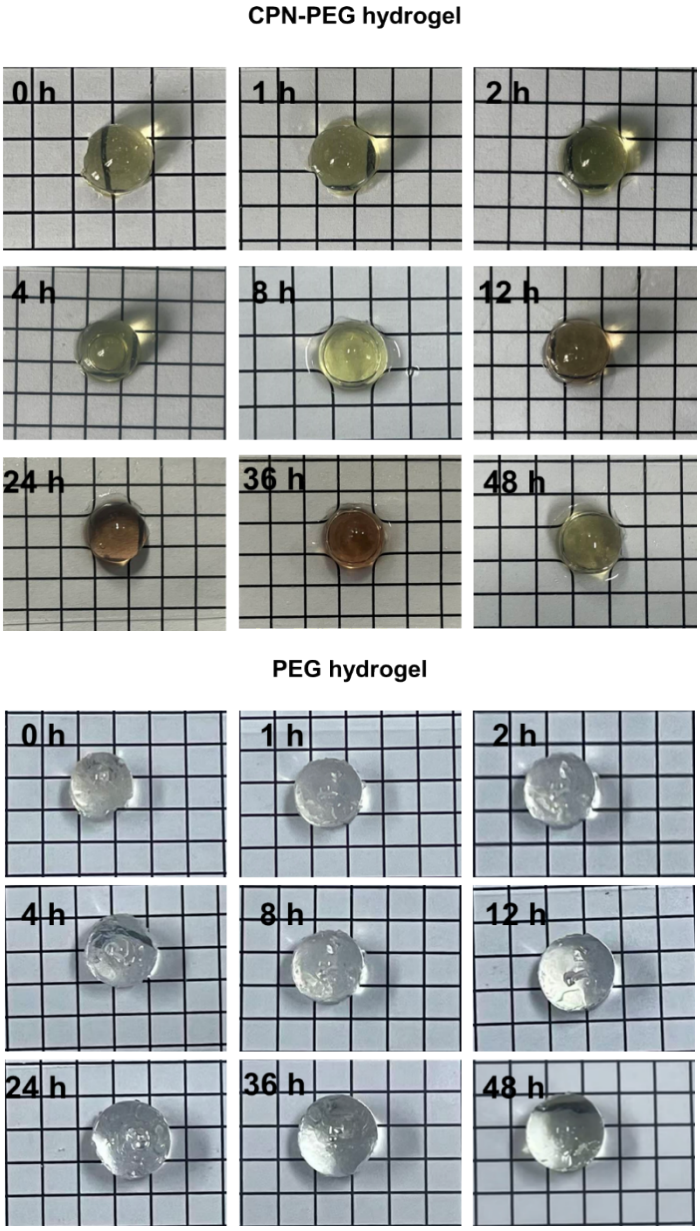

Figure S15. Swelling profiles of CPN-PEG hydrogel and PEG-hydrogel over a 48-hour period.

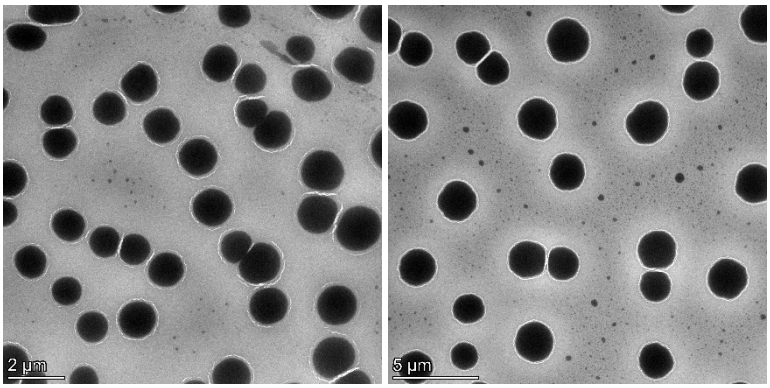

Figure S16. Transmission electron microscopy (TEM) images of the CPN-PEG hydrogel network.

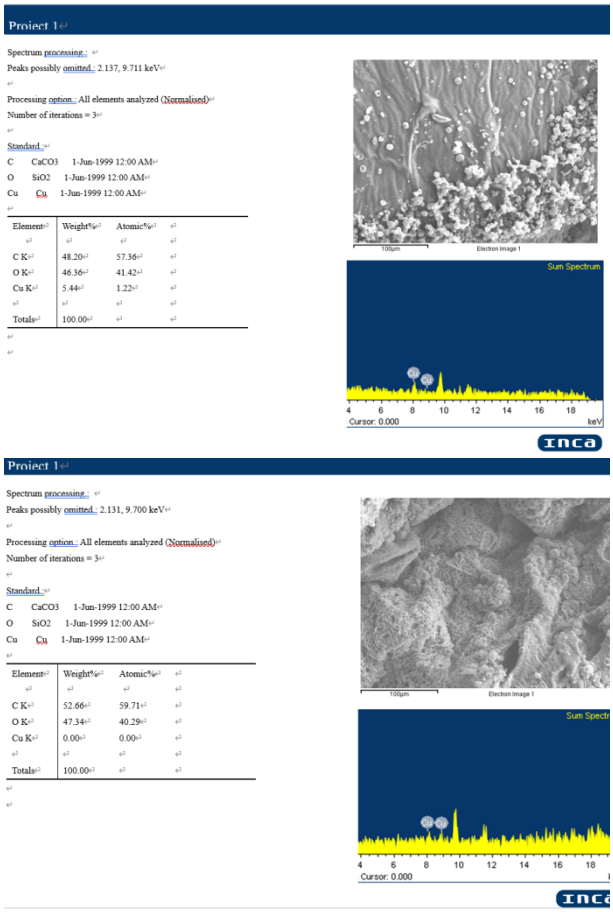

Figure S17. EDS spectra of the hydrogel surface before (top) and after (bottom) washing with EDTA and PBS.

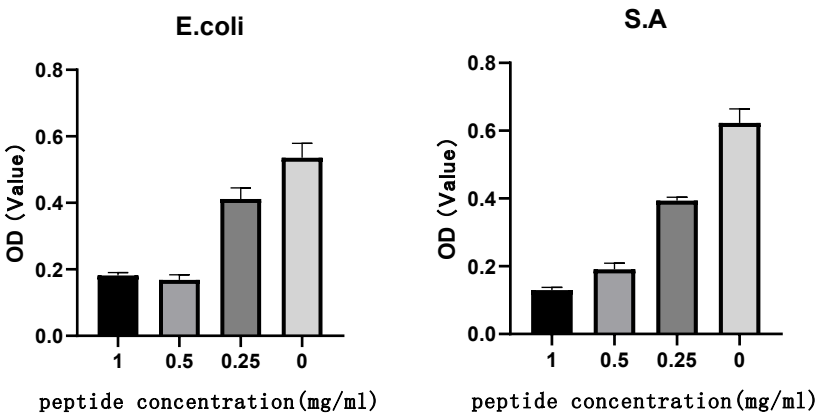

Figure S18. Antibacterial activity of the CP against E. coli and S. Aureus, quantified by OD_{600} measurements.

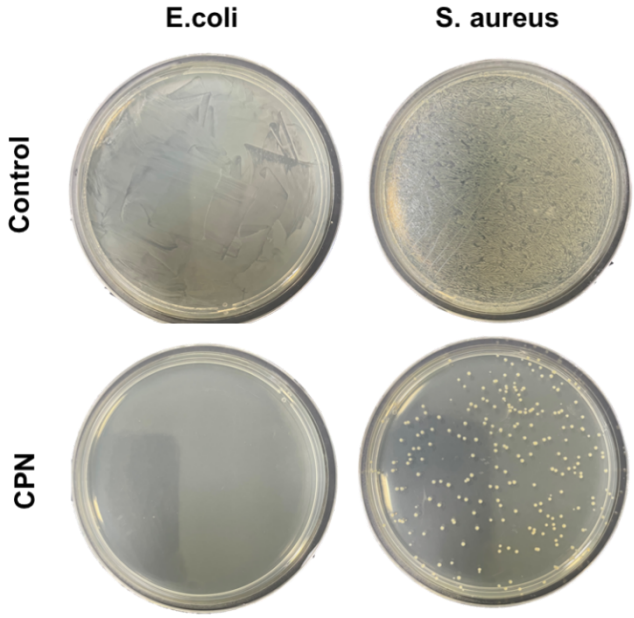

Figure S19. Antibacterial activity of the CPN against E. coli and S. Aureus by the spread plate method.

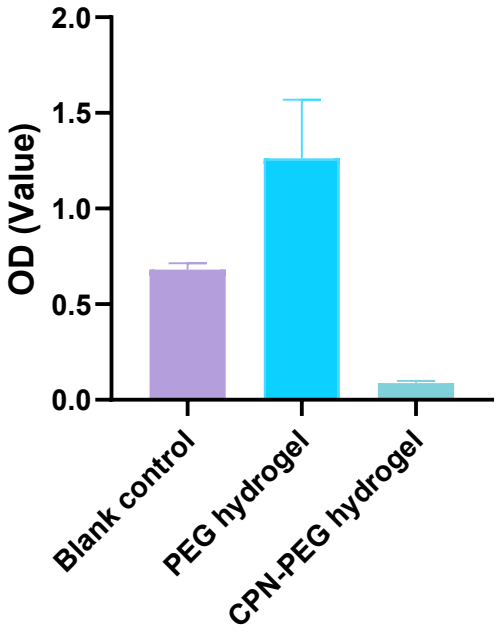

Figure S20. Antibacterial activity of the hydrogel against *E. coli*, quantified by OD_{600} measurements.

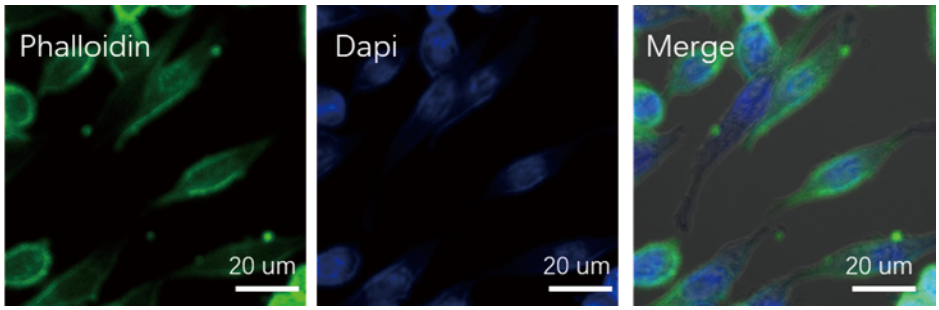

Figure S21. Viability and cytoskeletal integrity of L929 cells co-cultured with hydrogel extracts, as demonstrated by Phalloidin (for F-actin) and DAPI (for nuclei) staining.

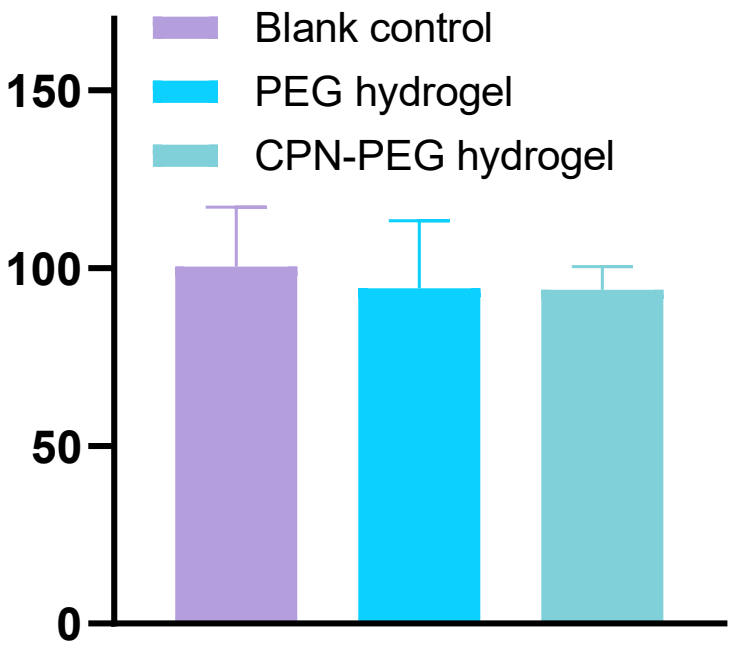

Figure S22. Viability of L929 cells co-cultured with CPN-PEG hydrogel, PEG-hydrogel, and the control group, assessed by CCK-8 assay.

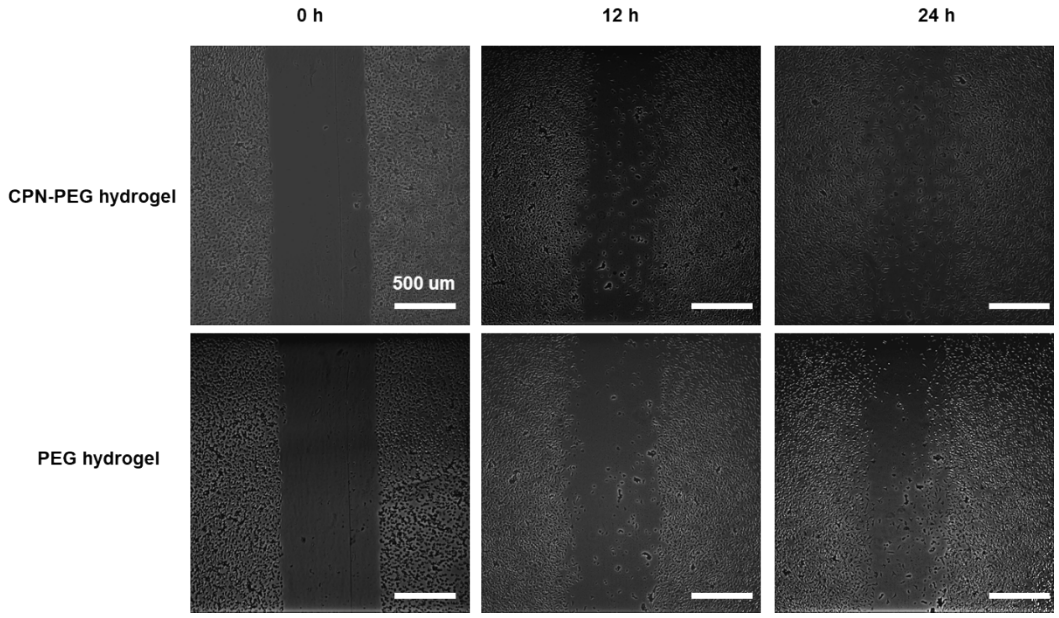

Figure S23. Cell migration of L929 cells after co-culture with CPN-PEG hydrogel and PEG-hydrogel extracts, assessed by scratch assay at 12 h and 24 h time points.

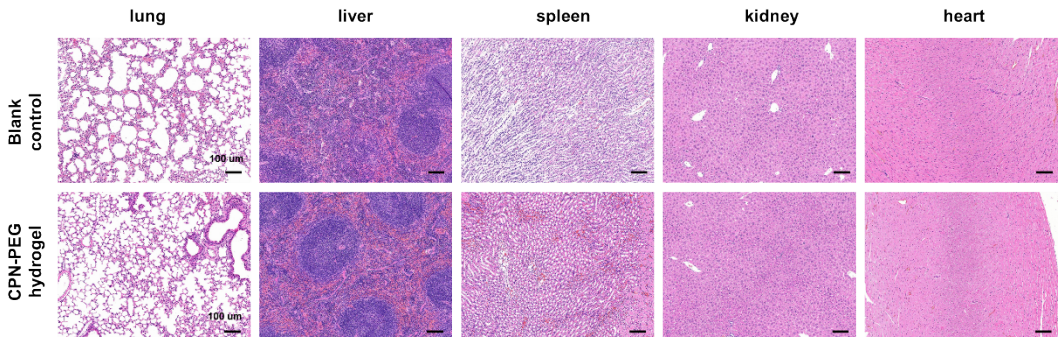

Figure S24. H&E staining of heart, liver, spleen, lung, and kidney sections from the blank control and CPN-PEG hydrogel groups after 12 days of experimentation.